67. H. Siomi, M. Choi, M. C. Siomi, R. L. Nussbaum, G. Dreyfuss, *Cell* **77**, 33 (1994).
68. K. De Boulle *et al.*, *Nat. Genet.* **3**, 31 (1993).
69. M. J. Matunis, W. M. Michael, G. Dreyfuss, *Mol. Cell. Biol.* **12**, 164 (1992); M. Takimoto *et al.*, *J. Biol. Chem.* **268**, 18249 (1993).
70. J. Engebrecht and G. S. Roeder, *Mol. Cell. Biol.* **10**, 2379 (1990); K. Nandabalan, L. Price, G. S. Roeder, *Cell* **73**, 407 (1993).
71. T. J. Gibson, P. M. Rice, J. D. Thompson, J. Heringa, *Trends Biochem. Sci.* **18**, 331 (1993).
72. R. L. Nussbaum and D. H. Ledbetter, in *Metabolic Basis of Inherited Disease*, C. R. Scriver, A. Beaudet, W. S. Sly, D. Valle, Eds. (McGraw-Hill, New York, ed. 7, in press).
73. R. J. Buckanovich, J. B. Posner, R. B. Darnell, *Neuron* **11**, 657 (1993).
74. D. St. Johnston, N. H. Brown, J. G. Gall, M. Jantsch, *Proc. Natl. Acad. Sci. U.S.A.* **89**, 10979 (1992).
75. S. R. Green and M. Mathews, *Genes Dev.* **6**, 2478 (1992); G. S. Fang, K. Chong, A. Kumar, B. R. Williams, *Proc. Natl. Acad. Sci. U.S.A.* **89**, 5447 (1992); B. L. Bass, S. R. Hurst, J. D. Singer, *Curr. Biol.* **4**, 301 (1994).
76. S. J. McCormack, D. C. Thomis, C. E. Samuel, *Virology* **188**, 47 (1992).
77. A. Gatignol, A. Buckler-White, B. Berkhout, K.-T. Jeang, *Science* **251**, 1597 (1991).
78. A. Gatignol, C. Buckler, K.-T. Jeang, *Mol. Cell. Biol.* **13**, 2193 (1993).
79. D. St Johnston *et al.*, *Cell* **66**, 51 (1991); D. St Johnston, W. Driever, T. Berleth, S. Richstein, C. Nüsslein-Volhard, *Development* **107** (suppl.), 13 (1989); A. Ephrussi, L. K. Dickinson, R. Lehmann, *Cell* **66**, 37 (1991); J. Kim-Ha, J. L. Smith, P. M. Macdonald, *ibid.*, p. 23; T. Berleth *et al.*, *EMBO J.* **7**, 1749 (1988).
80. M. B. Mathews and T. Shenk, *J. Virol.* **65**, 5657 (1991).
81. J. C. Watson, H.-W. Chang, B. L. Jacobs, *Virology* **185**, 206 (1991).
82. O. Theunissen, F. Rudt, U. Guddat, H. Mentzel, T. Pieler, *Cell* **71**, 679 (1992).
83. K. E. Joho, M. K. Darby, E. T. Crawford, D. D. Brown, *ibid.* **61**, 293 (1990).
84. G. Wistow, *Nature* **344**, 823 (1990).
85. S. R. Tafuri and A. P. Wolffe, *Trends Cell Biol.* **3**, 94 (1993).
86. R. D. Klausner, T. A. Rouault, J. B. Harford, *Cell* **72**, 19 (1993).
87. E. Chu *et al.*, *Proc. Natl. Acad. Sci. U.S.A.* **88**, 8977 (1991).
88. M. W. Hentze, *Trends. Biochem. Sci.* **19**, 101 (1994).
89. A. Sachs and E. Wahle, *J. Biol. Chem.* **268**, 22955 (1993).
90. W. C. Boelens *et al.*, *Cell* **72**, 881 (1993).
91. X.-D. Fu and T. Maniatis, *Science* **256**, 535 (1992).
92. H. Ge, P. Zuo, J. L. Manley, *Cell* **66**, 373 (1991); A. R. Krainer, A. Mayeda, D. Kozak, G. Binns, *ibid.*, p. 383; A. Mayeda and A. R. Krainer, *ibid.* **68**, 365 (1992).
93. Y. Takagaki, C. C. MacDonald, T. Shenk, J. L. Manley, *Proc. Natl. Acad. Sci. U.S.A.* **89**, 1403 (1992).
94. M. O. J. Olson, in *The Eukaryotic Nucleus: Molecular Biochemistry and Macromolecular Assemblies*, P. Strauss and S. Wilson, Eds. (Telford, Caldwell, NJ, 1990), vol. 2, p. 519.
95. O. Delattre *et al.*, *Nature* **359**, 162 (1992).
96. J. T. Anderson, S. M. Wilson, K. V. Datar, M. S. Swanson, *Mol. Cell. Biol.* **13**, 2730 (1993).

97. We thank members of our laboratory, I. Mattaj, and M. Malim for comments on the manuscript, and M. Görlach and D. Portman for assistance with the figures. Supported by grants from the National Institutes of Health and by the Howard Hughes Medical Institute.

Arctic Ocean Gravity Field Derived From ERS-1 Satellite Altimetry

Seymour Laxon and David McAdoo

The derivation of a marine gravity field from satellite altimetry over permanently ice-covered regions of the Arctic Ocean provides much new geophysical information about the structure and development of the Arctic sea floor. The Arctic Ocean, because of its remote location and perpetual ice cover, remains from a tectonic point of view the most poorly understood ocean basin on Earth. A gravity field has been derived with data from the ERS-1 radar altimeter, including permanently ice-covered regions. The gravity field described here clearly delineates sections of the Arctic Basin margin along with the tips of the Lomonosov and Arctic mid-ocean ridges. Several important tectonic features of the Amerasia Basin are clearly expressed in this gravity field. These include the Mendeleev Ridge; the Northwind Ridge; details of the Chukchi Borderland; and a north-south trending, linear feature in the middle of the Canada Basin that apparently represents an extinct spreading center that "died" in the Mesozoic. Some tectonic models of the Canada Basin have proposed such a failed spreading center, but its actual existence and location were heretofore unknown.

Persistent sea ice has kept surface research ships out of much of the Arctic Ocean. As a consequence, our understanding of Arctic Ocean Basin geology and geophysics lags well behind that of the other major ocean basins (*1*). On the basis of relatively abundant aeromagnetic surveys (*2, 3*) plus a limited amount of surface data (*4*), an uncertain tectonic history has been constructed for the oceanic Arctic Basin (*5*). Over ice-free oceans, data from satellite radar altimeters have been used with great success (*6, 7*) to determine marine gravity fields. These fields can help in determining the tectonic history of the ocean floor (*8*). Previous altimeter missions have covered areas below 72°N, but the ERS-1 satellite provides observations up to 82°N covering a large area of the Arctic Basin for the first time. The Arctic Basin is generally divided into two sub-basins: the Eurasia Basin and the Amerasia Basin, separated by the Lomosonov Ridge. The Amerasia Basin, whose tectonic history is particularly uncertain, is mostly covered by ERS-1 altimeter observations of sea ice. The presence of sea ice introduces unacceptable errors into the height estimate that is computed on board the satellite (*9*). In this article we present a gravity field for the Arctic Ocean, derived from data that have been corrected for on-board errors by reprocessing. We further validate our gravity field using surface observations and discuss the tectonic implications.

S. Laxon is at the Mullard Space Science Laboratory, Department of Space and Climate Physics, University College London, Holmbury Saint Mary, Dorking, Surrey RH5 6NT, UK. D. McAdoo is at the Geosciences Laboratory, Ocean and Earth Sciences, National Ocean Service, National Oceanic and Atmospheric Administration, Silver Spring, MD 20910, USA.

Tectonic History

Knowledge of the tectonic history of the Arctic Basin is key to understanding the role of the Arctic Ocean in past climate change. An accurate Arctic tectonic history is also needed to ensure accurate global tectonic models and to understand the geology of the Arctic continental margins (*10*).

The Arctic Basin is generally divided into two parts, each with a distinct plate-tectonic history: The smaller Eurasia Basin, which lies between Eurasia and the Lomonosov Ridge, was formed by sea floor spreading on the Arctic (Nansen) mid-ocean Ridge likely beginning 55 million years ago (Ma) (*11*). The Amerasia Basin (Fig. 1) represents the remaining two-thirds of the Arctic Basin, which probably formed in late Neocomian to Late Cretaceous time (~130 Ma) (*3, 4*), and has an uncertain tectonic history (*2, 5*). Of the many tectonic models proposed for the early development of the Amerasia Basin, the most widely held involve arctic Alaska rifting away from the Canadian arctic islands in the Mesozoic and rotating to its present position. This rotation is thought to have been accompanied by sea floor spreading that produced the ocean crust of the southern and central Canada Basin. However, the locus or axis of such sea floor spreading had not been found. Taylor and colleagues (*3*), on the basis of aeromagnetic profiles, speculate that an extinct spreading axis was located roughly in the middle of the southern Canada Basin. However, data from aeromagnetic surveys have since been considered inadequate to resolve this problem. Another possible source of the spreading is the Mendeleev–Alpha Cordillera Ridge (*2*).

Recent work (*12*) indicates that the Canadian end of the Alpha Ridge is volcanic in origin, but surface data have not been sufficient to rule out a spreading-center origin for the rest of the Alpha–Mendeleev Cordillera or to refute fully other speculations (*13*) that the Cordillera is a continental fragment or was formed above a subduction zone (*14*).

Satellite Gravity Over Sea Ice

The mean topography of the sea surface, be it open ocean or covered with sea ice, conforms to the geoid and therefore reflects variations in the Earth's gravity field. Long-wavelength variations of the field reflect density variations in the Earth's mantle and crust, whereas shorter wavelength (<250 km) features reflect the topography of the sea floor plus the density of the oceanic crust and uppermost mantle. Over ice-free oceans, data from satellite radar altimeters such as Geosat and Seasat have been used with great success to determine global marine gravity fields up to 72° latitude (*6, 15*). These altimetric gravity fields can be used to help map tectonic structures, fracture zones, active and extinct mid-ocean ridges, and propagating rifts (*8*). During the geodetic phase of the Geosat altimeter mission, where a high spatial density of tracks was acquired, gravity fields with spatial resolutions as high as 2 to 3 km were generated (*7, 16*). These fields are particularly useful in poorly mapped areas, such as the southern ocean, where ship surveying may be no better than a few hundred kilometers (*17*).

Because its orbit is more highly inclined (98°) than other altimeter satellites, the ERS-1 radar altimeter provides coverage of the Arctic up to 82°N. Gravity fields of ice-free areas in the Norwegian-Greenland sea have already been produced with ERS-1 altimetry (*18, 19*). Most data over the tectonically important Arctic Basin have,

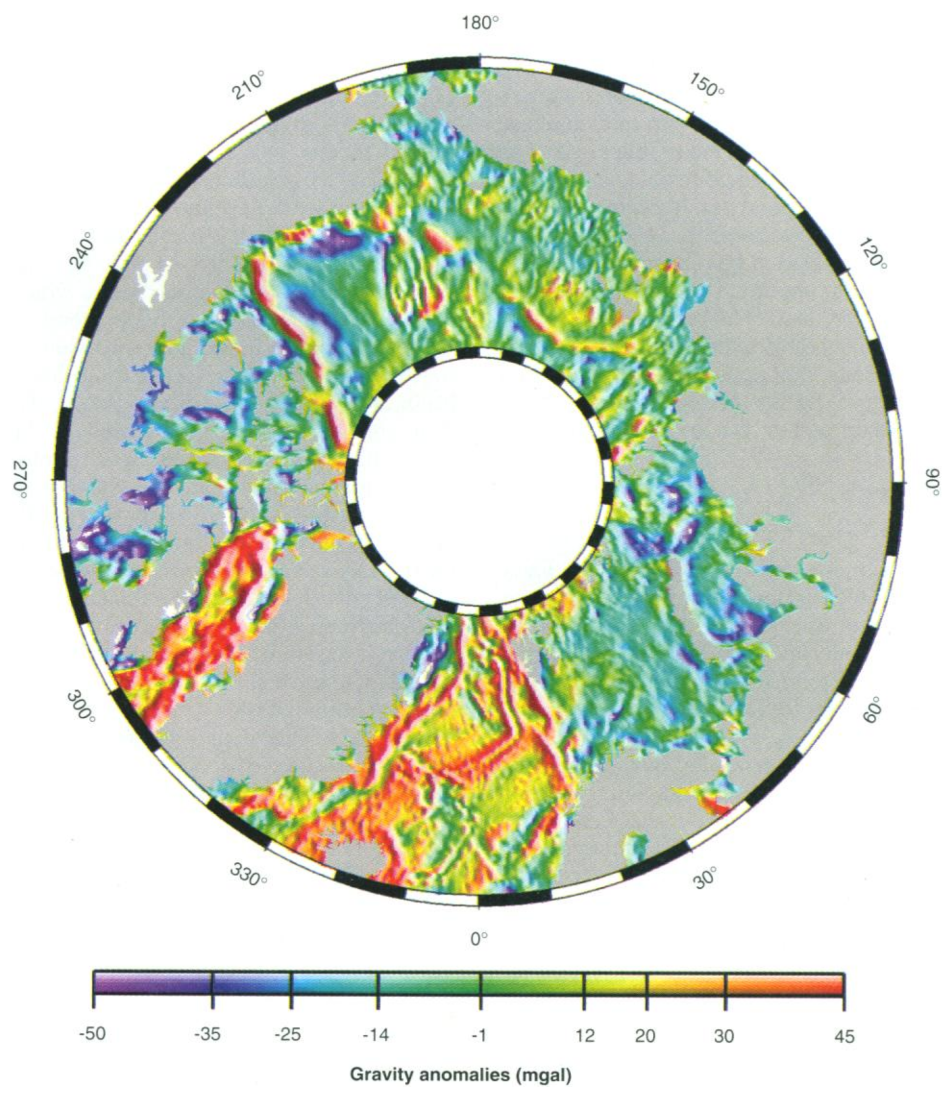

Fig. 1. (Top) Index and physiographic map for the Arctic Ocean. Depth contours (interval of 1000 m) are drawn from the National Oceanic and Atmospheric Administration–National Geophysical Data Center Global Gridded Elevation and Bathymetry database (ETOP05). NR, Northwind ridge; ChB, Chukchi borderland; MR, Mendeleev Ridge; AR, Alpha Ridge; LR, Lomonosov Ridge; AMOR, Arctic (Nansen) Mid-Ocean Ridge. The southern latitude limit is 64°N. The northern limit of ERS-1 coverage, latitude of 81.5°N, is plotted (inner circle). The shaded square in the Canada Basin shows the area in which densely spaced gravimetric observations taken on the sea ice are compared with our ERS-1 results. Note that much of the Eurasia Basin lies north of 81.5°N. **Fig. 2.** (Bottom) Gravity field of the Arctic Ocean from ERS-1 retracked altimetry over sea ice and open ocean. The image shown is a polar stereographic projection.

however, been excluded because of the presence of sea ice, which results in complex radar echoes (*20*) that confuse the on-board processor, resulting in much increased height noise (*21*).

To reduce this noise, it is necessary to reprocess the altimeter echoes recorded by the spacecraft. Reprocessing requires the use of the full-echo waveform data rather than the ocean product (OPR) data set, normally used for open-ocean gravity mapping, which contains only on-board estimates of surface height. By measuring the offset between the range given by the leading edge of the recorded echo and the range estimated by the on-board processor, a correction can be computed (*9*). When this correction is applied to the on-board estimates, the height noise is significantly reduced. After the removal of outliers and the elimination of spurious signals due to the ice cover, a Gaussian smoothing function is applied to the data, resulting in a smooth height profile from which along-track slopes can be computed. Gravity anomalies were then calculated for a single 35-day repeat cycle (cycle 96) from the method of McAdoo and Marks (*7*).

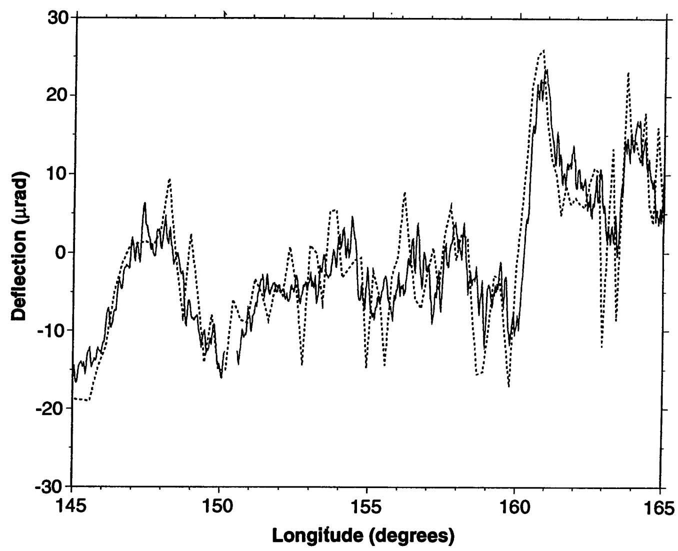

Fig. 3. Comparison between ERS-1 altimeter–derived deflections from the vertical during ice-covered (solid) and ice-free (dashed) periods. One microradian of vertical deflection corresponds to a gravity anomaly of approximately 0.98 mgal. Deflections for the ice-free profile are computed at 2 Hz with the ERS-1 altimeter ocean product (OPR), while the deflections for the ice-covered profile are computed at 20 Hz with the ERS-1 altimeter waveform product (WAP). The profile location AA′ is indicated in Fig. 1.

Results

The new data cover large areas that are permanently ice-covered and yield a gravity field for the Arctic Ocean from which tectonic details can be deduced. The resulting gravity field (Fig. 2) covers all ocean areas between 61°N and 82°N for the first time. A second, noisier repeat cycle was processed to ensure that the features appearing in Fig. 2 were not anomalous in origin.

Data that were obtained during a period of maximum ice retreat, when there was some open ocean, allowed a direct comparison between surface slopes derived with and without ice cover. The comparison (Fig. 3) shows a root-mean-square difference of ~5 μrad (corresponding to ~5 mgal) between slopes derived from the on-board estimates and those corrected during a period of ice cover corrected by return-echo analysis.

A comparison of our field with existing gravity surveys (*22, 23*) in the Beaufort Sea region is shown in Fig. 4. Overall there is excellent agreement, although some differences occur in coastal regions where some of the ERS-1 data have been deleted be-

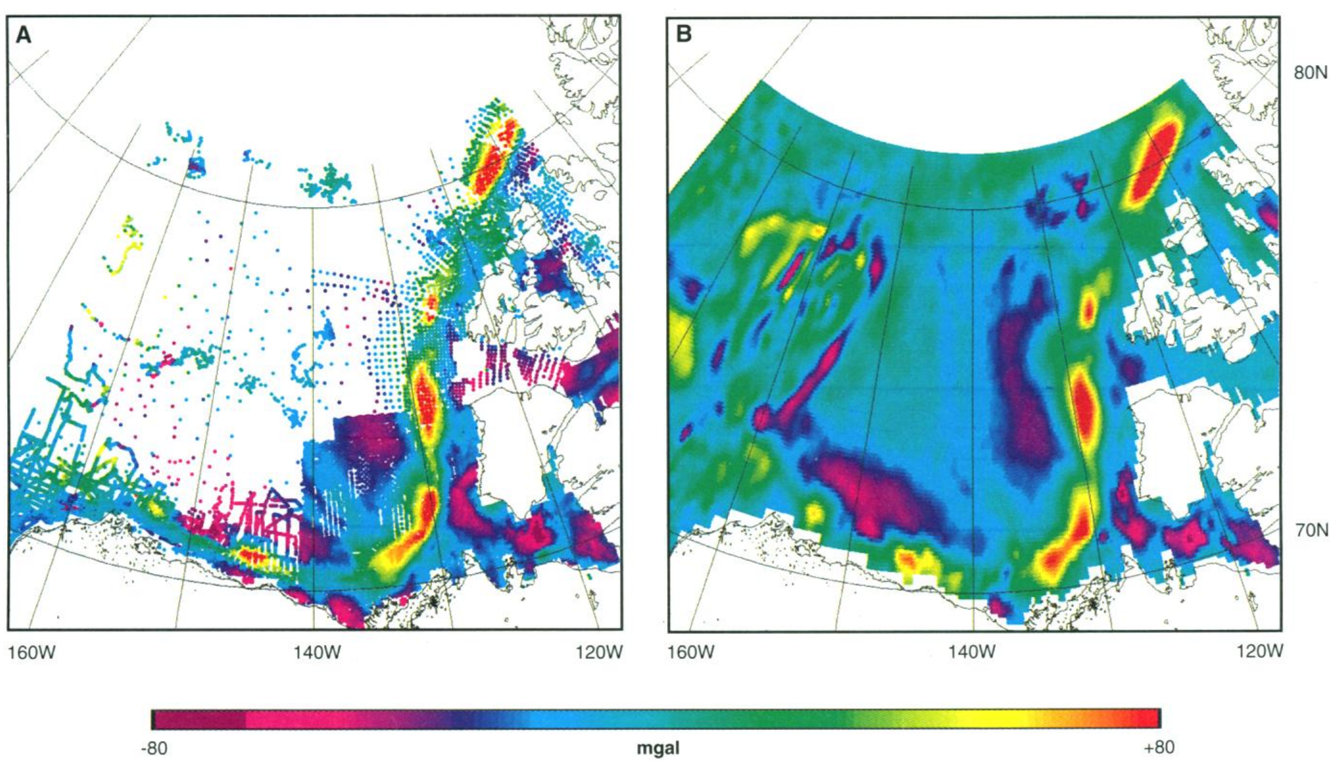

Fig. 4. (**A**) Surface gravity observations for the Beaufort Sea region. Densely spaced observations (in box) in the southwestern Beaufort were used for comparison with our ERS-1 gravity results. The image shown is an orthographic projection. (**B**) ERS-1 gravity field for the Beaufort Sea region. The image shown is an orthographic projection.

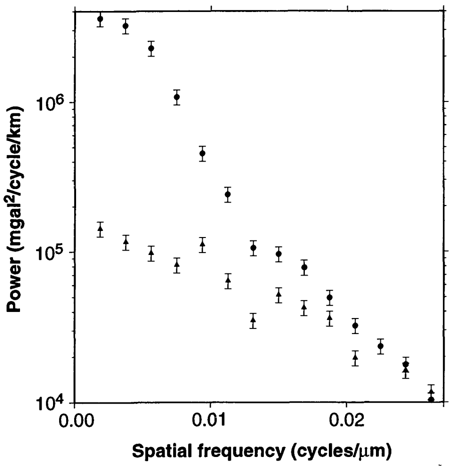

Fig. 5. Two-dimensional power spectra of the CGS surface gravimetry (circles) in a square area in the southeastern Beaufort Sea (see Figs. 1 and 4) and of the differences [or noise (triangles)] between surface gravimetry and ERS-1 gravity.

cause of coastal contamination. The Beaufort Sea, unlike most of the Arctic Ocean that is virtually unmapped by surface gravimetric observations, mapped well with observations from aircraft, ships, and drifting ice islands. A rectangular 500-km^2 area of the southernmost Beaufort Sea (compare Figs. 1 and 4) is particularly well mapped by gravimetric surveys taken on the sea ice. To estimate the accuracy and spatial resolution of our gravity field, we did a comparative analysis of the surface gravity results with our ERS-1 gravity results in this square area of the southeastern Beaufort Sea. We computed differences between the surface and ERS-1 gravity fields. We then estimated the two-dimensional power spectrum of the CGS surface gravity and a corresponding power spectrum of the differences or noise (Fig. 5). The point at which the power spectral density of the gravity signal equals that of the noise is taken as the short-wavelength limit of resolution, which we estimate to be ~75 km. The root-mean-square difference between the two gravity fields is 8 mgal, when error both in the ERS-1 derived gravity and in the CGS gravity measurement is taken into account.

Tectonic Interpretation

From the overall ERS-1 gravity field (Fig. 2), one can see tectonic fabric imprinted in the Arctic sea floor. The individual gravity anomalies correspond to both known and unknown tectonic or bathymetric features. The margins of the Arctic Basin, both the Amerasia and the Eurasia basins (Figs. 1 and 2), are clearly visible. Although much of the Eurasia Basin lies north of 82°N and is therefore unobserved, gravitational expression of the eastern tip of the Lomonosov Ridge (Fig. 1) and the Arctic (Nansen) Mid-Ocean Ridge (Fig. 1) can be seen in Fig. 2. In contrast to the Eurasia Basin, more than half of the enigmatic Amerasia Basin is imaged by our gravity map. A linear (purple) gravity low associated with the Northwind Ridge (Fig. 1) can be seen. Although seismic reflections (*4*) indicate that the Northwind is a site of Tertiary convergence but not subduction, this gravity low more closely resembles those at trenches and subduction zones elsewhere in the world's oceans. This Northwind low also looks similar to those observed over large-offset fracture zones such as the Eltanin fracture zone. Clearly, the Northwind is not a subduction zone and probably never was. Rather, it was more likely produced by compression across this edge of continental crust composing the Chukchi Borderland. Just west of the Northwind Ridge can be seen a complex of gravity anomalies that overlie the Chukchi Borderland (Fig. 1). Seismic reflection profiles (*4*) across the Chukchi Borderland suggest that it may be composed of continental crust that has undergone east-west extension. Indeed, the complex gravity anomalies that are revealed over the Chukchi may result from abandoned rift valleys or similar extensional structures. However, no evidence can be seen in Fig. 2 of a long Charlie transform fault, which has been postulated (*4*) to lie just north of the Chukchi Borderland. A linear feature roughly resembling fossil spreading ridges seen in Geosat gravity fields of the Southern Ocean can also be viewed in Fig. 2, roughly coincident with the Mendeleev Ridge (Fig. 1). The Mendeleev is largely unmapped by surface data; its exact nature is unknown, but some (*13*) have speculated that it may be a spreading center that died in the early Tertiary. Our gravity results may lead some researchers to speculate that this fossil spreading ridge hypothesis is valid. A linear gravity low over the extinct Aegir Ridge northeast of Iceland can be viewed in Fig. 2. Off the east coast of Greenland, a large negative anomaly overlying the outer continental shelf is observed. This low may result from residual crustal depression as a result of an enlarged, Early Holocene Greenland ice sheet or glacial erosion.

Perhaps the most tectonically significant feature in our gravity field is a north-south trending low at 142°W. This pattern suggests that an extinct spreading ridge underlies the thick sediments of the Canada Basin. This low is similar in appearance to that observed over the well-documented, extinct Aegir Ridge described above. At its southern end, this lineated gravity low appears to bend in a southeasterly direction toward the MacKenzie Delta. This pattern provides evidence that the Canada Basin was formed by the rotation of arctic Alaska away from the Canadian arctic islands and by consequent sea floor spreading about a pole in the MacKenzie Delta.

REFERENCES AND NOTES

1. A. Grantz, L. Johnson, J. F. Sweeney, Eds., *The Arctic Ocean Region*, Vol. L of *The Geology of North America* (Geological Society of America, Boulder, CO, 1990).
2. P. R. Vogt, P. T. Taylor, L. C. Kovacs, G. L. Johnson, *J. Geophys. Res.* **84**, 1071 (1979).
3. P. T. Taylor, L. C. Kovacs, P. R. Vogt, G. L. Johnson, *ibid.* **86**, 6323 (1981).
4. 1992 Arctic Summer West Scientific Party, *Eos* **74**, 249 (1993); *ibid.*, p. 253.
5. L. A. Lawver and C. R. Scotese, in (*1*), p. 593.
6. D. T. Sandwell and W. H. F. Smith, *Global Marine Gravity Field from ERS-1, Geosat and Seasat* (Scripps Institute of Oceanography, La Jolla, CA, 1992).
7. D. C. McAdoo and K. M. Marks, *J. Geophys. Res.* **97**, 3247 (1992).
8. D. T. Sandwell, "U.S. National Report to International Union of Geodesy and Geophysics 1987-1990," *Rev. Geophys.* (suppl.), 132 (1991).
9. S. Laxon, *Int. J. Remote Sensing* **15**, 915 (1994).
10. J. F. Sweeney, G. L. Johnson, A. Grantz, in (*1*), pp. 619–626.
11. L. A. Lawver, R. D. Muller, S. P. Srivastavar, W. Roest, in *The Geological History of the Polar Oceans: Arctic Versus Antarctic*, U. Bleil and J. Thiede, Eds. (Kluwer Academic, Dordrecht, Netherlands, 1990), pp. 29–62.
12. A. Grantz, S. D. May, P. T. Taylor, L. A. Lawver, in (*1*), pp. 379–402.
13. P. Vogt and N. A. Ostenso, *J. Geophys. Res.* **75**, 4925 (1970).
14. E. M. Herron, J. F. Dewey, W. C. Pitman III, *Geology* **2**, 377 (1974).
15. W. Haxby, *N.O.A.A. Gravity Field of the World's Oceans* (1987).
16. D. T. Sandwell, *Geophys. J. Inter.* **109**, 437 (1992).
17. T. H. Dixon and M. E. Parke, *Nature* **304**, 406 (1983).
18. P. Knudsen, O. B. Andersen, K. Matrikelstyrelsen, C. Tscherning, *Geophys. Res. Lett.* **19**, 1795 (1992).
19. A. J. Anderson, D. T. Sandwell, G. Marquart, H. G. Scherneck, "Space at the Service of Our Environment," *Proceedings of the First ERS-1 Symposium*, Cannes, France, 4 to 6 November 1992 (European Space Agency, ESA Document SP-359, Noordwijk, Netherlands, 1993), vol. 1, p. 463.
20. G. Q. Robin, *Philos. Trans. R. Soc. London Ser. A* **309**, 447 (1983).
21. C. G. Rapley, *Nature* **307**, 150 (1984).
22. L. W. Sobczak *et al.*, in (*1*), pp. 101–118.
23. Surface gravity data supplied by the Canadian Geophysical Survey.

24. We thank the European Space Agency; the U.K. Processing and Archiving Facility for providing the data; C. Rapley for providing encouragement and, along with K. Marks and F. Strawbridge, for providing critical review; J. Mansley for data preparation; and L. Daghorn for help in preparing the manuscript. Supported in part by a joint National Environment Research Council–Science and Engineering Research Council grant.